ACS APPLIED MATERIALS & INTERFACES

www.acsami.org Research Article

In-Fiber Polymer Microdisk Resonator and Its Sensing Applications of Temperature and Humidity

Peng Ji, Meng Zhu, Changrui Liao,* Cong Zhao, Kaiming Yang, Cong Xiong, Jinli Han, Chi Li, Lichao Zhang, Yifan Liu, and Yiping Wang

Cite This: *ACS Appl. Mater. Interfaces* 2021, 13, 48119−48126 Read Online

ABSTRACT: We proposed and realized an all-in-fiber polymer microdisk whispering-gallery mode (WGM) resonator, which is composed of a nanoscale polymer waveguide in conjunction with a polymer microdisk. The resonator is manufactured by femtosecond laser-induced two-photon polymerization inside a single-mode optical fiber, and its transmission spectrum has been investigated theoretically and experimentally. The WGM resonance was excited successfully, exhibiting a high Q factor of 2.3×10^3 at a resonant wavelength of 1416.6 nm. The temperature and humidity responses of the resonator were tested as examples of possible application. Temperature sensitivity of −96 pm/°C when the temperature increased from 25 to 60 °C and humidity sensitivity of 54 pm/%RH when the relative humidity increased from 30 to 90% were obtained. The proposed in-fiber microdisk resonator is highly suitable for detection of microorganisms, bacteria, and single molecules.

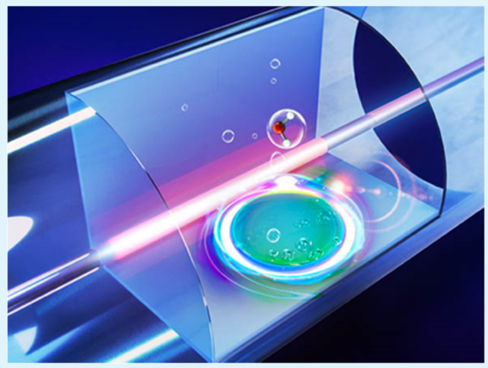

KEYWORDS: *polymer resonator, whispering-gallery mode, two-photon polymerization, optical fiber sensing, temperature sensing, humidity sensing*

1. INTRODUCTION

Because of their extremely narrow mode linewidths, extremely high photon state densities, extremely strong mode light energies, and high-quality factors, whispering-gallery mode (WGM) microcavities are widely employed in low-threshold lasers, high-sensitivity sensors, optical filters, nonlinear optics, and other applications.[1−5] In recent decades, WGM microcavities based on polymeric, semiconductor, and crystalline materials have been studied widely.[6−9] For sensing applications, the sensitivity of WGM resonators depends on several factors, such as the structure, size, material, noise, and experimental setup.[10,11] Among these, polymer-based WGMs, in particular, have been pursued and enable to provide higher sensitivity because of their beneficial physical and chemical properties, such as high elasticity and thermo-optical coefficient, simple surface modification/postmodification, and good plasticity and biocompatibility.[12−14] However, the complex excitation and detection devices required for WGM resonators lack flexibility for use in practical applications. Therefore, a more flexible and robust way to realize high-efficiency excitation and detection of WGM signals is being sought.

Recently, on-chip polymer microring/disk/toroid WGM resonators have been intensively investigated owing to their planar geometry and ease of fabrication. However, an additional coupling fiber or a fiber taper with a narrow waist is usually used for WGM excitation.[10,14−16] This configuration is fragile, encounters alignment issues, and may be affected by external airflow or contaminants. Alternatively, fiber optic approaches exhibit a suite of prominent merits, which include compact size, high flexibility, capable of alignment-free integration, and easy connection with optical fiber systems.[17−20] Therefore, direct integration of the WGM resonator with an optical fiber represents one ingenious way to achieve this goal. In 2015, Shi et al. fabricated a microdisk WGM resonator in an optical fiber by direct femtosecond (fs) laser ablation, while its Q factor is significantly limited by the surface roughness.[21] In 2018, Wang et al. realized a WGM resonator by directly embedding barium titanate glass microspheres into the air hole of a tapered hollow annular core fiber, and excited various WGMs via changing the resonator size and location.[22] Subsequently, Mallik et al. demonstrated two fiber-tip hybrid resonators based on silica microspheres coated with different polymer layers for multiparameter sensing, and their WGMs were excited simultaneously with the help of an external fiber taper.[23] Wei et al. proposed a polymer microring resonator for ultrasound detection, which was connected to a single-mode

Received: July 30, 2021
Accepted: September 15, 2021
Published: September 29, 2021

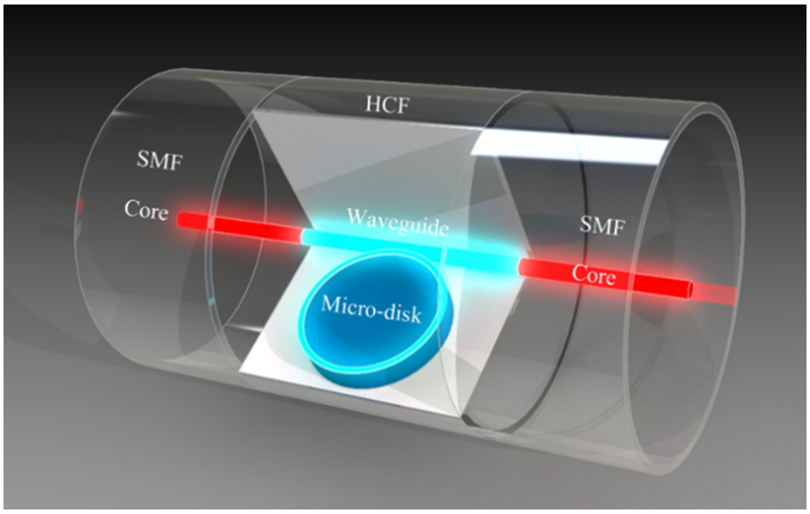

Figure 1. Schematic diagram of the proposed in-fiber polymer microdisk WGM resonator.

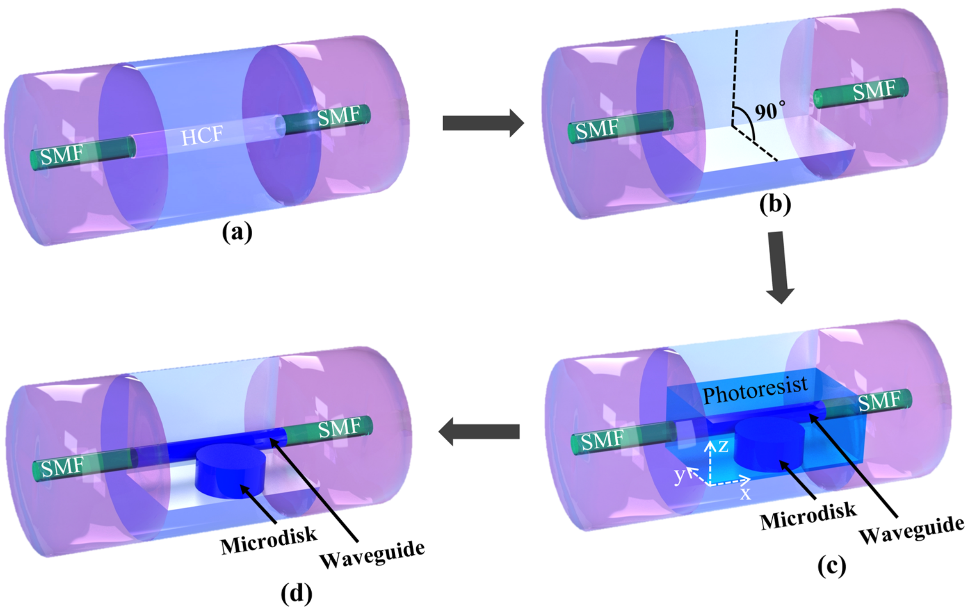

Figure 2. Flow diagram of the device fabrication process. (a) Short HCF section is spliced between two SMFs. (b) Angled platform (90°) is ablated in the HCF using a fs laser micromachining technique. (c) PR is fully filled into the platform and the designed nanoscale waveguide and the microdisk are then printed via TPP. (d) Uncured PR is cleaned and removed using a mixed solution of acetone and isopropanol.

fiber (SMF) using a curable optical adhesive and aligned by a five-dimensional positioning stage.[24] To further simplify the experimental setup, in 2019, Markiewicz et al. pasted two SMFs side by side and directly printed a polymer WGM resonator on the fiber end face.[25] Similarly, by replacing a pair of SMFs with a multicore fiber, a polymer WGM resonator on the end face of a multicore optical fiber was printed for vapor sensing.[19,20] Nevertheless, integration of a high-quality WGM resonator into a conventional SMF is a very significant and challenging task.

In this work, we propose a hollow-core fiber (HCF) internally integrated polymer microdisk WGM resonator composed of a polymer waveguide and a polymer microdisk that is printed by fs laser-induced two-photon polymerization (TPP). In terms of geometry, as illustrated in Figure 1, both the waveguide and the microdisk are well integrated within a single optical fiber, realizing an ingenious combination of the polymer WGM resonator and the optical fiber. The polymer waveguide connects the cores of SMFs on both sides to transmit optical signals and is particularly designed in nanometer size to provide a sufficiently large evanescent field. The polymer microdisk is in very close proximity to the waveguide and operates as a resonator cavity. The light propagating in the waveguide will be partly coupled into the microdisk through the evanescent wave of the nanoscale waveguide and excite WGMs in the resonator. A high Q factor of 2.3×10^3 at a wavelength of 1416.6 nm is achieved by taking advantage of the smooth surface of the fs laser-polymerized architecture. The optical characteristics of resonators with various sizes, refractive indices, and gap spacings are evaluated by a numerical simulation. Its sensing performance of temperature and humidity has also been studied experimentally as a preliminary attempt.

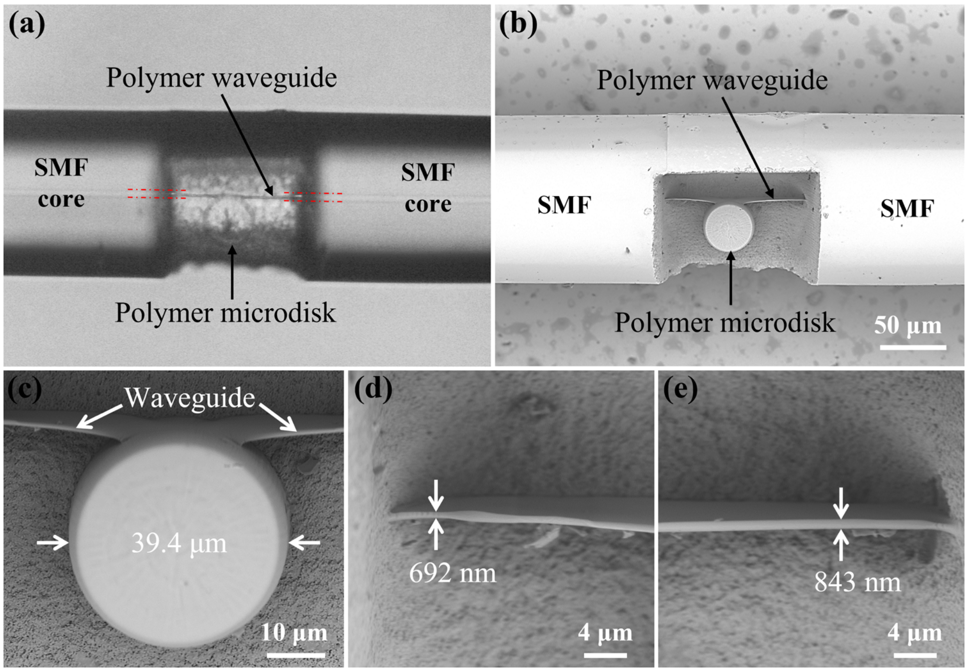

Figure 3. Top ($x-y$ plane) view of the fs laser-printed microdisk WGM resonator comprising a polymer waveguide and a polymer microdisk in an SMF. (a) Optical microscopy image. (b) SEM image of the entire resonator and details of the (c) microdisk and (d) waveguide on the left side and (e) right side.

2. DEVICE FABRICATION

Figure 2 shows the device fabrication process, which can be divided into the following four steps. First, a section of 130 μm HCF (internal/external diameters = 9/125 μm, respectively) is spliced between two thin-core SMFs (internal/external diameters = 3.8/125 μm, respectively), as shown in Figure 2a. The HCF is notably utilized to obtain two smooth interfaces at the SMF cores, which is pivotal to reduce of the connection loss between the polymer waveguide and the SMF. The sample is then fixed on a glass slide using an ultraviolet-curable adhesive to keep the fiber sample both straight and unstressed. Second, the HCF is ablated precisely using the focused fs laser beam to open a 90°-angled platform for polymer microstructure fabrication, as illustrated in Figure 2b. The bottom of the platform is designed to be located 15 μm lower than the height of the SMF core. After fs laser ablation, the fiber sample must be washed in an ultrasonic cleaning process to remove residual debris from the platform. Third, a photoresist (PR) is fully filled into the platform and covered using a standard cover slide. The PR used in this experiment is a negative resin (type: PP-1; purchased from Zhichu Optics Co., Ltd., Shenzhen, China), and its material composition is elaborated in ref 18. The dispersion of the PR material in the wavelength range from 1507 to 1615 nm was measured in our previous work.[26] The fs laser pulses used in this process have a central wavelength of 1026 nm, a pulse width of 250 fs, a repetition rate of 200 kHz, and a pulse energy of 12 nJ and are focused using a 50× objective (numerical aperture NA = 0.42) during laser polymerization.

The fiber sample on the glass slide is mounted on a three-dimensional (3D) air-bearing translation stage (Aerotech, ABL1500) with an accuracy of ±200 nm, as shown in Figure S1a, which allows precise positioning of the fiber sample and translation in accordance with the predetermined path and velocity. To ensure that the printed polymer waveguide is in good alignment with the fiber core on each side, with the help of a top-view vision system, each core is reliably aligned in relation to the focused laser beam with an accuracy of ∼500 nm. Under this condition, as indicated in Figure S1b, the fs laser beam can be precisely focused on the interface at the fiber core as the starting point for processing, and laser scanning is then carried out along the aligned path to form the polymer architecture. As shown in Figure 2c, the polymer microdisk is printed in a layer-by-layer polymerization manner on the surface of the platform from bottom to top along the z-axis. The height of the microdisk is 25 μm, and the slicing step is set to 500 nm, which is implemented by a servo controller (Aerotech Inc.) and its corresponding software (SCA lntro v2.6). The polymer waveguide is subsequently printed using a single scan with the same velocity of 200 μm/s. The waveguide must be very close to the microdisk to excite the WGM resonance efficiently. After laser polymerization, the printed structure is immersed in a developer solution (acetone and isopropanol mixture with a volume ratio of 1:4) for 2 min to remove any uncured PR and obtain the designed polymer microstructure, as illustrated in Figure 2d.

An optical microscopy image and a scanning electron microscopy (SEM) image of the top ($x-y$ plane) view of the microdisk WGM resonator fabricated inside an SMF are shown in Figure 3a,b, respectively. The details of the microdisk, nanoscale waveguide on the left side, and waveguide on the right side are given in Figure 3c−e, respectively. As presented in Figure 3a,b, the straight polymer waveguide is connected correctly to the cores of the SMFs on both sides and is perfectly tangential to the polymer microdisk. The length of the polymer waveguide is measured to be 128 μm.

Figure 3c shows that the waveguide is slightly fused into the microdisk and supported by it, which helps to improve mechanical stability.[23] For sensing applications, it has been demonstrated that the environment-induced refractive index (RI) change is more significant than the geometric deformation.[11,15] Therefore, it has a minor effect on the sensing performance. The diameter of the polymer microdisk is measured to be 39.4 μm, and a very smooth surface can be observed, which is essential for realizing the high-quality factor of the WGM resonator. Figure 3d,e show that the polymer waveguide is tightly attached to the sidewalls of the laser-ablated fiber. Owing to the large depth of focus of the 50× objective, the height of the waveguide is approximately 10 μm, which, in turn, helps to support the waveguide by the bottom fiber cladding and enhances the robustness of the printed architecture. The polymer waveguide is slightly bent and deformed, with thickness varying from ∼700 to ∼850 nm. This is mainly because the waveguide is printed in the suspended state, and during the last cleaning step, it is difficult to avoid the suspended polymer waveguide being bent and attached to the microdisk as a result of volatilization and surface tension of the cleaning solution.[24] The optical guiding properties of the waveguide are also simulated, and the result is presented in Figure S2, where transverse electric (TE) and transverse magnetic (TM) modes are well confined. Generally, the printed structure is consistent with the theoretically designed structure and the structure's size deviation is acceptable. The laser printing accuracy is affected by several factors, including the performance of the translation stage, the TPP parameters, and the cleaning method used.

3. NUMERICAL SIMULATIONS

When broad-band light is coupled from the left SMF into the nanoscale polymer waveguide, a strong waveguide evanescent field will be generated. When the integral multiple of the wavelength is equal to the optical path length of the microdisk, the light corresponding to that wavelength will stably exist and excite WGM resonance on the microdisk. The relationship between the parameters of the microdisk and the resonant wavelength is given by

$$\pi n d = m\lambda \tag{1}$$

where n and d denote the effective RI and the diameter of the microdisk, respectively. The effective RI of the polymer material used in this work is ∼1.543 (at λ = 1507 nm), which is much higher than that of silica to ensure light guiding inside the polymer layer.[26,27] λ is the resonant wavelength of the light and m is the azimuthal number, which is a positive integer. From eq 1, the free spectral range (FSR) of the WGM resonance can be deduced to be

$$\mathrm{FSR} = \frac{\lambda^2}{\pi d n} \tag{2}$$

The Q factor is a key parameter of the WGM resonator. It represents the light energy storage property of the resonator and is defined as $Q = \lambda/\Delta\lambda$, where $\Delta\lambda$ denotes the full width at half-maximum (FWHM) of the wavelength.

To better understand its optical characteristics, the microdisk WGM resonator with different gap spacings (g), RIs (n), and diameters (d) is estimated using FDTD Solutions, a commercially available modeling tool based on the finite-difference time-domain method. The calculation results are shown in Figure 4a−c. In the simulation, it is simply assumed that the polymer material has no material dispersion, the waveguide width is 900 nm, and the gap spacing between the waveguide and the microdisk is defined as g. For the case of g = 0, the waveguide is just in contact with the microdisk.

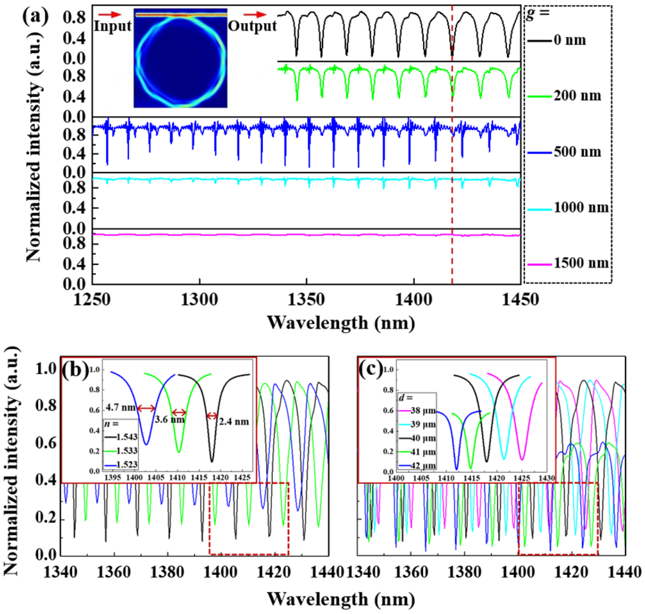

Figure 4. Calculated transmission spectra of the microdisk WGM resonator with various (a) gap spacings of g = 0 to 1500 nm, (b) RIs of n = 1.523 to 1.543, and (c) diameters of d = 38 to 42 μm. The top insets of (a)−(c) show the mode field at λ = 1417.7 nm and the Lorentzian fitting curves of the corresponding WGM resonance appearing in the red dashed box, respectively.

Figure 4a plots the calculated transmission spectra of the microdisk WGM resonator when g = 0 to 1500 nm, while maintaining d = 40 μm and n = 1.543. The inset of Figure 4a shows the mode field at a resonant wavelength of 1417.7 nm when g = 0. It is observed that the light propagates in the waveguide and is also partly coupled into the microdisk through the evanescent wave of the nanoscale waveguide that causes further excitation of the WGM resonance on the microdisk, while the mode field is mainly distributed in the boundary. The modulation depth, defined as the intensity contrast at the resonant dip, is observed to drop sharply from 0.893 to 0.049 when g increases from 0 to 1000 nm, by virtue of the attenuated evanescent field and resulting in less coupling between the waveguide and the microdisk. For g = 500 and 1000 nm, the WGM resonance of the fundamental mode is suppressed as g increases, however, its resonance of high order mode is remarkably enhanced. For g > 1000 nm, there are almost no interactions between the mode in the microdisk and that in the waveguide, thus no excited WGM resonance in the transmission spectrum. This might be attributed to the leakage of all coupled modes on the microdisk as a result of surface scattering.[21] Nevertheless, the resonant wavelength is almost steady, exhibiting a negligible wavelength shift, which is less than 1 nm. Furthermore, for the case of g = 0, the calculated FSR at 1417.7 nm is 12.3 nm.

Figure 4b plots the calculated transmission spectra of n in the range of 1.523 to 1.543, given d = 40 μm and g = 0. As presented in the inset of Figure 4b of the Lorentzian fitting curve, the resonant wavelength shifts toward shorter wavelengths and modulation depth reduces with decreasing n, which is in good agreement with the prediction based on eq 1. The resonant wavelength and the modulation depth for n = 1.543, 1.533, and 1.523 are (1417.9 nm, 1410.3 nm, 1402.7 nm) and (0.906, 0.812, 0.736), respectively, exhibiting a ratio of wavelength shift to RI of 760 nm/RIU. On top of the blue-

https://doi.org/10.1021/acsami.1c14499
ACS Appl. Mater. Interfaces 2021, 13, 48119−48126

shifted wavelength and reduced optical intensity, the bandwidth of the transmission spectrum broadens with decreasing n to deteriorate the Q factor. The corresponding $\Delta\lambda$ is 2.4, 3.6, and 4.7 nm, respectively.

Moreover, as plotted in Figure 4c, the effect of d on the resonant characteristics is also simulated when $n = 1.543$ and $g = 0$. The inset of Figure 4c shows the Lorentzian fitting curve of the corresponding WGM resonance appearing in the red dashed box, where the wavelength is in the range of 1400 to 1430 nm. The resonant wavelength shifts to shorter wavelengths when d increases from 38 to 42 μm, while the FSR and bandwidth are both shrunken, providing an improved Q factor. This illuminates that the optical mode coupling between the waveguide and the microdisk is rarely affected by d, and the excited WGM resonance corresponds to different azimuthal numbers of m = 129, 133, 137, 140, and 144, respectively, for d = 38 to 42 μm.

4. EXPERIMENTAL RESULTS AND DISCUSSION

Figure 5 shows the measured transmission spectrum of the prepared all-in-fiber polymer microdisk WGM resonator with a designed diameter of $d = 40$ μm, using a broad-band light source (FiberLake, ASE-1250-1650) and an optical spectrum analyzer (Yokogawa, AQ6370C). In the spectrum, multiple resonances, as well as nonuniform modulation depth can be observed, indicating multimode interference of the transmitted signal in the polymer waveguide. This is because the polymer waveguide itself constructed in SMF also constitutes a Fabry−Perot interferometer, which typically generates multimode interference, as elaborated in our previous work.[26] The insertion loss was measured to be as large as 20 dB; this loss mainly results from mode-field mismatch and RI differences between the polymer waveguide and the silica SMFs on both sides. However, the insertion loss can be reduced by printing tapers at both ends of the straight polymer waveguide to overcome the mode-field mismatch. The FSR at λ = 1416.6 nm was 11.5 nm, which differs slightly from the measured value in Figure 4; this may be the result of RI differences caused by material dispersion and dimensional errors in the micromachining of the structure. The Q factor was calculated to be 2.3×10^3 at λ = 1416.6 nm, which is lower than that of conventional silica WGM resonators. The low Q factor may result from a comprehensive effect, such as the absorption loss of the polymer material,[14] the imperfect surface roughness of the microdisk,[21] and the overcoupling between the waveguide and the microdisk,[16,28] which are in contact with each other. But it can be improved by annealing the polymer microdisk to improve its surface quality or changing to another PR with lower light absorption.

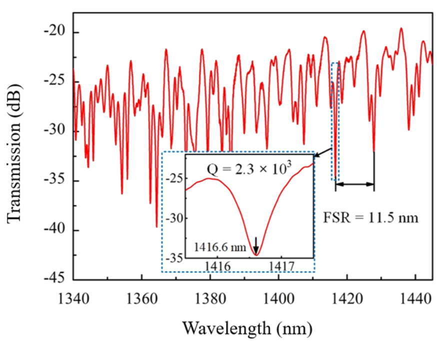

Figure 5. Experimental transmission spectrum of the prepared in-fiber polymer WGM microdisk resonator, which has a diameter of d = 40 μm.

The WGM resonators are highly sensitive to the surrounding medium and have been widely used in various sensing applications. When compared with silica, most polymer materials have higher thermo-optic and thermal expansion coefficients, which is favorable for temperature sensor applications. The temperature response of the prepared WGM resonator has thus been investigated experimentally. During the test, the device was placed in a column oven with a temperature accuracy of 0.1 °C. The temperature was gradually increased from 25 to 60 °C in steps of 5 °C and maintained for 20 min in each step (at 55% RH). The resonant dip at a wavelength of 1416.6 nm was used to monitor temperature changes.

Figure 6a shows the transmission spectra acquired at different temperatures. As the temperature increases, the spectra are shown to shift toward shorter wavelengths (blue shift) and the modulation depth of the resonant dip declines dramatically. For the case of 60 °C, the WGM resonance is quite weak because the WGM excited by the evanescent field of the nanoscale waveguide almost leaks out of the microdisk due to surface scattering,[21] as described above in Figure 4a. Simultaneously, the bandwidth of the transmission spectrum broadens with increasing surrounding temperature to deteriorate the Q factor. This can be the result of the reduced RI of the polymer as temperature increases,[26] which is consistent with the analytical calculation in Figure 4b. Furthermore, since the polymer may soften when heated, the contact points of the polymer waveguide and the SMF cores, as well as the microdisk may be slightly separated as temperature increases, resulting in an increase in coupling loss, thereby weakening the WGM resonance. The relationship between the dip wavelength and the oven temperature is depicted in Figure 6b, where a good linear response with a sensitivity of −96 pm/°C was obtained. As temperature increased from 25 to 60 °C, the resonant dip shifts from 1417.89 to 1414.46 nm, with a wavelength shift of 3.43 nm, which corresponds to an RI change of 4.51×10^{-3} according to the calculation in Figure 4b. To quantify the range of temperature sensitivity, a similar test was carried out using a different microdisk WGM resonator S1, and the experimental results are shown in Figure S3a,b, providing a sensitivity of −95 pm/°C.

Theoretically, the wavelength shift ($\Delta\lambda'$) of the resonant dip caused by the temperature change can be described by[29]

$$\Delta\lambda' = \lambda[\frac{1}{n}\cdot\frac{\mathrm{d}}{\mathrm{d}T}(n)\cdot\Delta T + \frac{1}{d}\cdot\frac{\mathrm{d}}{\mathrm{d}T}(d)\cdot\Delta T] \quad (3)$$

where ΔT is the temperature change, $\mathrm{d}(n)/\mathrm{d}T$ is the thermo-optic coefficient of the polymer (of the order of -10^{-4} K^{-1}), and $\mathrm{d}(d)/\mathrm{d}T$ is the thermal expansion coefficient of the polymer, which has a positive value. In the experiment, the resonance spectrum exhibits a blue shift with increasing temperature, demonstrating that the thermo-optic effect is more significant than the thermal expansion effect and thus plays a dominant role in the spectrum shift. Assuming that there is no thermal expansion effect, the thermo-optic coefficient for RI change with temperature is calculated to be -1.07×10^{-4} K^{-1}.

In addition to temperature-sensing applications, polymer-based devices also offer great advantages in humidity sensing. Therefore, the humidity response of the prepared WGM resonator was hereby explored. Before the experiment, the sample was first placed in a drying oven for 24 h (relative humidity of 20%, temperature of 21°C), and a humidity sensing experiment was then performed at a constant temperature of 25 °C. The test chamber humidity slowly increased from 30 to 90% in steps of 10% and each humidity state was maintained for 20 min to ensure that the humidity in the test chamber was sufficiently stable. The resonant dip at the same wavelength of 1416.6 nm was used to monitor humidity changes. Figure 6c shows the spectral evolution when the ambient humidity increased from 30 to 90%, which demonstrates that the spectra shift toward longer wavelengths (red shift). In addition, contrary to the temperature response, the modulation depth and bandwidth of the transmission spectrum get higher and narrower as the humidity increases, respectively, rendering an improved Q factor. This is because when the humidity increases, the polymer material will absorb the water molecules to increase its RI.[30] Moreover, the diameter of the polymer microdisk will also increase because of polymer swelling caused by water absorption.[31] Both mechanisms lead to the red shift of the transmission spectrum, while it has been proved that the RI effect in polymer materials is two orders of magnitude higher than the

https://doi.org/10.1021/acsami.1c14499
ACS Appl. Mater. Interfaces 2021, 13, 48119−48126

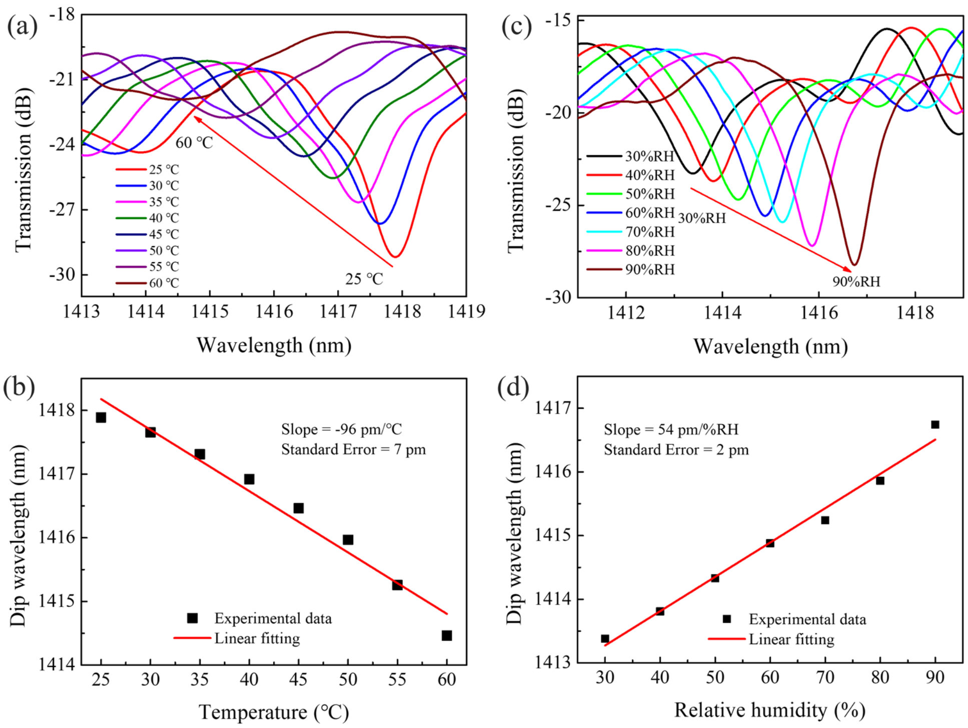

Figure 6. (a) Spectral evolution of the prepared in-fiber microdisk WGM resonator with increasing temperature from 25 to 60 °C. (b) Linear fit of the dip wavelength versus temperature. (c) Spectral evolution of the prepared in-fiber microdisk WGM resonator with increasing ambient humidity from 30 to 90%. (d) Linear fit of the dip wavelength versus ambient humidity characteristics.

diameter effect,[15] especially for the non-free-standing configurations, where the microdisk is fully attached to the rigid supporting substrate.[31] Therefore, for the proposed WGM resonator, RI changes are the leading mechanism that affects the humidity response. The relationship between the dip wavelength and the ambient humidity is shown in Figure 6d, in which the dip wavelength shows a good linear response to the ambient humidity and a sensitivity of 54 pm/%RH, which is competitive in the previously reported polymer WGM resonators.[30,32] In addition, we tested the humidity response with another device S2 under the same conditions, as shown in Figure S3c,d, exhibiting a sensitivity of 55 pm/%RH. As humidity increased from 30 to 90%, the wavelength shift is 3.36 nm and an RI change of 4.42×10^{-3} is thus predicted. Similar to the thermo-optic coefficient, the hygroscopic coefficient for RI change with humidity is calculated to be 6.10×10^{-5} $\%RH^{-1}$, which is basically consistent with the previous report based on an SU-8 polymer.[15]

5. CONCLUSIONS

In summary, we have demonstrated an all-in-fiber polymer microdisk WGM resonator fabricated using fs laser-induced TPP technology. When compared with previously reported optical fiber-based WGM resonators, the greatest virtue of the proposed device is that both the waveguide and the microdisk are integrated well within a conventional silica optical fiber. This method realizes a perfect combination of the WGM resonator and the optical fiber and provides a flexible and robust way for efficiently exciting and detecting WGM signals. A comprehensive numerical calculation has been carried out for the WGM resonator with various dimensions, RIs, and gap spacings to provide insight into the influence of the Q factor. A high Q factor of 2.3×10^3 has been achieved by taking advantage of the smooth surface of the fs laser-polymerized architecture. As examples of possible application, the sensing performance of the resonator has been studied experimentally and temperature sensitivity of −96 pm/°C and humidity sensitivity of 54 pm/%RH were obtained. This all-in-fiber polymer microdisk resonator, which is ultracompact in size and highly integrated within an optical fiber, may find further promising applications in fields including optical fiber sensors and optical communication devices.

■ ASSOCIATED CONTENT

Supporting Information

The Supporting Information is available free of charge at https://pubs.acs.org/doi/10.1021/acsami.1c14499.

Experimental setup for preparing the in-fiber polymer microdisk resonator, simulated guiding modes of the printed nanoscale waveguide, and spectral evolution of additional polymer microdisk resonator S1 and S2 (PDF)

■ AUTHOR INFORMATION

Corresponding Author

Changrui Liao − *Key Laboratory of Optoelectronic Devices and Systems of Ministry of Education/GuangDong Province, College of Physics and Optoelectronic Engineering, Shenzhen University, Shenzhen 518060, China; Shenzhen Key Laboratory of Photonic Devices and Sensing Systems for Internet of Things, Guangdong and Hong Kong Joint Research Centre for Optical Fibre Sensors, Shenzhen University, Shenzhen 518060, China;* orcid.org/0000-0003-3669-5054; Email: cliao@szu.edu.cn

Authors

Peng Ji − *Key Laboratory of Optoelectronic Devices and Systems of Ministry of Education/GuangDong Province, College of Physics and Optoelectronic Engineering, Shenzhen University, Shenzhen 518060, China; Shenzhen Key*

Laboratory of Photonic Devices and Sensing Systems for Internet of Things, Guangdong and Hong Kong Joint Research Centre for Optical Fibre Sensors, Shenzhen University, Shenzhen 518060, China

Meng Zhu − *Key Laboratory of Optoelectronic Devices and Systems of Ministry of Education/GuangDong Province, College of Physics and Optoelectronic Engineering, Shenzhen University, Shenzhen 518060, China; Shenzhen Key Laboratory of Photonic Devices and Sensing Systems for Internet of Things, Guangdong and Hong Kong Joint Research Centre for Optical Fibre Sensors, Shenzhen University, Shenzhen 518060, China*

Cong Zhao − *Key Laboratory of Optoelectronic Devices and Systems of Ministry of Education/GuangDong Province, College of Physics and Optoelectronic Engineering, Shenzhen University, Shenzhen 518060, China; Shenzhen Key Laboratory of Photonic Devices and Sensing Systems for Internet of Things, Guangdong and Hong Kong Joint Research Centre for Optical Fibre Sensors, Shenzhen University, Shenzhen 518060, China*

Kaiming Yang − *Key Laboratory of Optoelectronic Devices and Systems of Ministry of Education/GuangDong Province, College of Physics and Optoelectronic Engineering, Shenzhen University, Shenzhen 518060, China; Shenzhen Key Laboratory of Photonic Devices and Sensing Systems for Internet of Things, Guangdong and Hong Kong Joint Research Centre for Optical Fibre Sensors, Shenzhen University, Shenzhen 518060, China*

Cong Xiong − *Key Laboratory of Optoelectronic Devices and Systems of Ministry of Education/GuangDong Province, College of Physics and Optoelectronic Engineering, Shenzhen University, Shenzhen 518060, China; Shenzhen Key Laboratory of Photonic Devices and Sensing Systems for Internet of Things, Guangdong and Hong Kong Joint Research Centre for Optical Fibre Sensors, Shenzhen University, Shenzhen 518060, China;* orcid.org/0000-0003-4621-9270

Jinli Han − *Key Laboratory of Optoelectronic Devices and Systems of Ministry of Education/GuangDong Province, College of Physics and Optoelectronic Engineering, Shenzhen University, Shenzhen 518060, China; Shenzhen Key Laboratory of Photonic Devices and Sensing Systems for Internet of Things, Guangdong and Hong Kong Joint Research Centre for Optical Fibre Sensors, Shenzhen University, Shenzhen 518060, China*

Chi Li − *Key Laboratory of Optoelectronic Devices and Systems of Ministry of Education/GuangDong Province, College of Physics and Optoelectronic Engineering, Shenzhen University, Shenzhen 518060, China; Shenzhen Key Laboratory of Photonic Devices and Sensing Systems for Internet of Things, Guangdong and Hong Kong Joint Research Centre for Optical Fibre Sensors, Shenzhen University, Shenzhen 518060, China*

Lichao Zhang − *Key Laboratory of Optoelectronic Devices and Systems of Ministry of Education/GuangDong Province, College of Physics and Optoelectronic Engineering, Shenzhen University, Shenzhen 518060, China; Shenzhen Key Laboratory of Photonic Devices and Sensing Systems for Internet of Things, Guangdong and Hong Kong Joint Research Centre for Optical Fibre Sensors, Shenzhen University, Shenzhen 518060, China*

Yifan Liu − *Key Laboratory of Optoelectronic Devices and Systems of Ministry of Education/GuangDong Province, College of Physics and Optoelectronic Engineering, Shenzhen University, Shenzhen 518060, China; Shenzhen Key Laboratory of Photonic Devices and Sensing Systems for Internet of Things, Guangdong and Hong Kong Joint Research Centre for Optical Fibre Sensors, Shenzhen University, Shenzhen 518060, China*

Yiping Wang − *Key Laboratory of Optoelectronic Devices and Systems of Ministry of Education/GuangDong Province, College of Physics and Optoelectronic Engineering, Shenzhen University, Shenzhen 518060, China; Shenzhen Key Laboratory of Photonic Devices and Sensing Systems for Internet of Things, Guangdong and Hong Kong Joint Research Centre for Optical Fibre Sensors, Shenzhen University, Shenzhen 518060, China*

Complete contact information is available at: https://pubs.acs.org/10.1021/acsami.1c14499

Author Contributions

P.J. and M.Z. contributed equally. P.J., M.Z., and C. Liao jointly conceived the idea. P.J. and M.Z. designed and fabricated the devices, built the experimental setup, and performed the experiments. P.J., M.Z., C.Z., K.Y., C.X., J.H., and C. Li analyzed the data. L.Z., Y.L., and Y.W. assisted with the theory. P.J. and M.Z. wrote the manuscript with contributions from all co-authors. All authors have given approval to the final version of the manuscript.

Notes

The authors declare no competing financial interest.

■ ACKNOWLEDGMENTS

The authors are grateful for financial supports from the National Natural Science Foundation of China (NSFC) (62075136, 62005173), the Natural Science Foundation of Guangdong Province (2018B030306003, 2020A0505100066), the Science and Technology Innovation Commission of Shenzhen (JCYJ20200109114001806, JCYJ20180507184503128, JCYJ20190808161019406), and the Postdoctoral Science Foundation of China (2018M643162).

■ REFERENCES

(1) Yan, D. D.; Shi, T. C.; Zang, Z. G.; Zhao, S. Y.; Du, J.; Leng, Y. X. Stable and Low-Threshold Whispering-Gallery-Mode Lasing from Modified $CsPbBr_3$ Perovskite Quantum Dots@SiO_2 Sphere. *Chem. Eng. J.* **2020**, *401*, No. 126066.

(2) Li, J.; Lu, Y.; Cao, L.; Li, M.; Song, Y. J. Continuously Tunable Fiber Laser Based on Fano Resonance Filter of Thin-Fiber-Taper-Coupled Conical Microresonator. *Opt. Commun.* **2020**, *466*, No. 125629.

(3) Guo, Z. H.; Qin, Y. C.; Chen, P. Z.; Hu, J. L.; Zhou, Y.; Zhao, X. Y.; Liu, Z. R.; Fei, Y. Y.; Jiang, X. S.; Wu, X. Hyperboloid-Drum Microdisk Laser Biosensors for Ultrasensitive Detection of Human Igg. *Small* **2020**, *16*, No. 2000239.

(4) Feng, Y. M.; Zheng, Y. L.; Zhang, F. X.; Yang, J. F.; Qin, T.; Wan, W. J. Passive Fine-Tuning of Microcavity Whispering Gallery Mode for Nonlinear Optics by Thermo-Optical Effect. *Appl. Phys. Lett.* **2019**, *114*, No. 101103.

(5) Zheng, Y.; Wu, Z. F.; Shum, P. P.; Xu, Z. L.; Keiser, G.; Humbert, G.; Zhang, H. L.; Zeng, S. W.; Dinh, X. Q. Sensing and Lasing Applications of Whispering Gallery Mode Microresonators. *Opto-Electron. Adv.* **2018**, *1*, No. 180015.

(6) Cai, M.; Painter, O.; Vahala, K. J. Observation of Critical Coupling in a Fiber Taper to a Silica-Microsphere Whispering-Gallery Mode System. *Phys. Rev. Lett.* **2000**, *85*, 74−77.

https://doi.org/10.1021/acsami.1c14499
ACS Appl. Mater. Interfaces 2021, 13, 48119−48126

(7) He, L. N.; Özdemir, S. K.; Zhu, J. G.; Kim, W. S.; Yang, L. Detecting Single Viruses and Nanoparticles Using Whispering Gallery Microlasers. *Nat. Nanotechnol.* **2011**, *6*, 428−432.

(8) Humar, M.; Ravnik, M.; Pajk, S.; Muševič, I. Electrically Tunable Liquid Crystal Optical Microresonators. *Nat. Photonics* **2009**, *3*, 595−600.

(9) Lee, H. S.; Chen, T.; Li, J.; Yang, K. Y.; Jeon, S. M.; Painter, O.; Vahala, K. J. Chemically Etched Ultrahigh-Q Wedge-Resonator on a Silicon Chip. *Nat. Photonics* **2012**, *6*, 369−373.

(10) Mehrabani, S.; Kwong, P.; Gupta, M.; Armani, A. M. Hybrid Microcavity Humidity Sensor. *Appl. Phys. Lett.* **2013**, *102*, No. 241101.

(11) Foreman, M. R.; Swaim, J. D.; Vollmer, F. Whispering Gallery Mode Sensors. *Adv. Opt. Photon.* **2015**, *7*, 168−240.

(12) Markos, C.; Stefani, A.; Nielsen, K.; Rasmussen, H. K.; Yuan, W.; Bang, O. High-Tg TOPAS Microstructured Polymer Optical Fiber for Fiber Bragg Grating Strain Sensing at 110 Degrees. *Opt. Express* **2013**, *21*, 4758−4765.

(13) Smith, M. J.; Zeng, Q. J.; Lafalce, E.; Yu, S. T.; Zhang, S. D.; Vardeny, Z. V.; Tsukruk, V. V. Coupled Whispering Gallery Mode Resonators via Template-Assisted Assembly of Photoluminescent Microspheres. *Adv. Funct. Mater.* **2019**, *29*, No. 1902520.

(14) Wu, J. S.; Guo, X.; Zhang, A. P.; Tam, H. Y. Rapid 3D μ-Printing of Polymer Optical Whispering-Gallery Mode Resonators. *Opt. Express* **2015**, *23*, 29708−29714.

(15) Eryürek, M.; Tasdemir, Z.; Karadag, Y.; Anand, S.; Kilinc, N.; Alaca, B. E.; Kiraz, A. Integrated Humidity Sensor Based on SU-8 Polymer Microdisk Microresonator. *Sens. Actuators, B* **2017**, *242*, 1115−1120.

(16) Kelemen, L.; Lepera, E.; Horvath, B.; Ormos, P.; Osellame, R.; Vazquez, R. M. Direct Writing of Optical Microresonators in a Lab-on-a-Chip for Label-Free Biosensing. *Lab Chip* **2019**, *19*, 1985−1990.

(17) Wang, R. H.; Fraser, M.; Li, J. C.; Qiao, X. G.; Wang, A. B. Integrated In-Fiber Coupler for Microsphere Whispering-Gallery Modes Resonator Excitation. *Opt. Lett.* **2015**, *40*, 308−311.

(18) Liao, C. R.; Li, C.; Wang, C.; Wang, Y.; He, J.; Liu, S.; Bai, Z. Y.; Gan, Z. S.; Wang, Y. P. High-Speed All-Optical Modulator Based on a Polymer Nanofiber Bragg Grating Printed by Femtosecond Laser. *ACS Appl. Mater. Interfaces* **2020**, *12*, 1465−1473.

(19) Zhang, S. Y.; Tang, S. J.; Feng, S. F.; Xiao, Y. F.; Cui, W. Y.; Wang, X. K.; Sun, W. F.; Ye, J. S.; Han, P.; Zhang, X. P.; Zhang, Y. High-Q Polymer Microcavities Integrated on a Multicore Fiber Facet for Vapor Sensing. *Adv. Opt. Mater.* **2019**, *7*, No. 1900602.

(20) Liu, Q. Q.; Zhan, Y. X.; Zhang, S. Y.; Feng, S. F.; Wang, X. K.; Sun, W. F.; Ye, J. S.; Zhang, Y. "Optical Tentacle" of Suspended Polymer Micro-Rings on a Multicore Fiber Facet for Vapor Sensing. *Opt. Express* **2020**, *28*, 11730−11741.

(21) Shi, L. L.; Zhu, T.; Huang, D. M.; Liu, M.; Deng, M.; Huang, W. In-Fiber Whispering-Gallery-Mode Resonator Fabricated by Femtosecond Laser Micromachining. *Opt. Lett.* **2015**, *40*, 3770−3773.

(22) Wang, J. W.; Zhang, X. B.; Yan, M.; Yang, L.; Hou, F. Y.; Sun, W.; Zhang, X. T.; Yuan, L. B.; Xiao, H.; Wang, T. Y. Embedded Whispering-Gallery Mode Microsphere Resonator in a Tapered Hollow Annular Core Fiber. *Photon. Res.* **2018**, *6*, 1124−1129.

(23) Mallik, A. K.; Farrell, G.; Ramakrishnan, M.; Kavungal, V.; Liu, D.; Wu, Q.; Semenova, Y. Whispering Gallery Mode Micro Resonators for Multi-Parameter Sensing Applications. *Opt. Express* **2018**, *26*, 31829−31838.

(24) Wei, H.; Krishnaswamy, S. Polymer Micro-Ring Resonator Integrated with a Fiber Ring Laser for Ultrasound Detection. *Opt. Lett.* **2017**, *42*, 2655−2658.

(25) Markiewicz, K.; Wasylczyk, P. Photonic-Chip-on-Tip: Compound Photonic Devices Fabricated on Optical Fibers. *Opt. Express* **2019**, *27*, 8440−8445.

(26) Li, C.; Liao, C. R.; Wang, J.; Li, Z. Y.; Wang, Y.; He, J.; Bai, Z. Y.; Wang, Y. P. Femtosecond Laser Microprinting of a Polymer Fiber Bragg Grating for High-Sensitivity Temperature Measurements. *Opt. Lett.* **2018**, *43*, 3409−3412.

(27) Xiong, C.; Zhou, J. T.; Liao, C. R.; Zhu, M.; Wang, Y.; Liu, S.; Li, C.; Zhang, Y. F.; Zhao, Y. Y.; Gan, Z. S.; Venturelli, L.; Kasas, S.; Zhang, X. M.; Dietler, G.; Wang, Y. P. Fiber-Tip Polymer Microcantilever for Fast and Highly Sensitive Hydrogen Measurement. *ACS Appl. Mater. Interfaces* **2020**, *12*, 33163−33172.

(28) Fang, Z. W.; Lin, J. T.; Wang, M.; Liu, Z. M.; Yao, J. P.; Qiao, L. L.; Cheng, Y. Fabrication of a Microresonator-Fiber Assembly Maintaining a High-Quality Factor by CO_2 Laser Welding. *Opt. Express* **2015**, *23*, 27941−27946.

(29) Zhang, X. B.; Xiong, J. B.; Gu, F.; Li, J. L.; Wang, W. Y.; Pang, F. F.; Wang, T. Y. Fabrication and Sensing Characteristics of Intrinsic Fabry-Perot Interferometers in Fiber Tapers. *Chin. Opt. Lett.* **2015**, *13*, 120602−120605.

(30) Xu, W.; Xu, C. X.; Qin, F. F.; Shan, Y. Q.; Zhu, Z.; Zhu, Y. Whispering-Gallery Mode Lasing from Polymer Microsphere for Humidity Sensing. *Chin. Opt. Lett.* **2018**, *16*, No. 081401.

(31) Lemieux-Leduc, C.; Guertin, R.; Bianki, M. A.; Peter, Y. A. All-Polymer Whispering Gallery Mode Resonators for Gas Sensing. *Opt. Express* **2021**, *29*, 8685−8697.

(32) Huang, Q. L.; Xu, H. L.; Li, M. T.; Hou, Z. S.; Lv, C.; Zhan, X. P.; Li, H. L.; Xia, H.; Wang, H. Y.; Sun, H. B. Stretchable PEG-DA Hydrogel-Based Whispering-Gallery-Mode Microlaser with Humidity Responsiveness. *J. Lightwave Technol.* **2018**, *36*, 819−824.

https://doi.org/10.1021/acsami.1c14499
ACS Appl. Mater. Interfaces 2021, 13, 48119−48126